Laser writing of nonlinear optical properties in silver-doped phosphate glass.

Evgeniya Smetanina, Benoit Chimier, Yannick Petit, Arnaud Royon, Thierry Cardinal, Lionel Canioni, Guillaume Duchateau

▶ **To cite this version:**

Evgeniya Smetanina, Benoit Chimier, Yannick Petit, Arnaud Royon, Thierry Cardinal, et al.. Laser writing of nonlinear optical properties in silver-doped phosphate glass.. Optics Letters, 2017, 42 (9), pp.1688-1691. 10.1364/OL.42.001688 . hal-01519733

HAL Id: hal-01519733
https://hal.science/hal-01519733

Submitted on 11 Mar 2021

HAL is a multi-disciplinary open access archive for the deposit and dissemination of scientific research documents, whether they are published or not. The documents may come from teaching and research institutions in France or abroad, or from public or private research centers.

L'archive ouverte pluridisciplinaire **HAL**, est destinée au dépôt et à la diffusion de documents scientifiques de niveau recherche, publiés ou non, émanant des établissements d'enseignement et de recherche français ou étrangers, des laboratoires publics ou privés.

Laser Writing of Nonlinear Optical Properties in silver-doped phosphate glass

E.O. SMETANINA[1,*], B. CHIMIER[1], Y. PETIT[1,2], A. ROYON[2], T. CARDINAL[2], L. CANIONI[1], AND G. DUCHATEAU[1]

[1] Université de Bordeaux-CEA-CNRS, Centre Lasers Intenses et Applications, UMR 5107, F-33405 Talence, France
[2] ICMCB, UPR 9048 CNRS, Université de Bordeaux, F-33608 Pessac, France
[*] Corresponding author: evgeniya.smetanina@u-bordeaux.fr

Compiled October 6, 2016

The formation of both local second and third harmonic generations (SHG and THG) induced by a train of femtosecond laser pulses in silver-doped phosphate glasses is addressed. Based on modeling calculations including various diffusion and kinetic processes, THG is shown to result from the formation of silver clusters. The latter organize into a ring-shape structure leading to the emergence of a static electric field. By breaking the glass centro-symmetry, this field gives rise to a local effective second order susceptibility inducing SHG. Both theoretically predicted SHG and THG evolutions with respect to the number of pulses in the train are in a good agreement with experimental observations. In particular, the observed reaching of a maximum in the nonlinear optical responses after a few thousands of pulses is explained by the competition of various physical processes.

OCIS codes: *(140.3390) Laser materials processing; (140.6810) Thermal effects; (160.6990) Transition-metal-doped materials; (160.4330) Nonlinear optical materials; (190.4720) Optical nonlinearities of condensed matter.*

http://dx.doi.org/XX.XXXX/XX.XX.XXXXXX

Femtosecond laser processing of glasses doped with metal ions provides the possibility for controllable formation of color centers, metal particles, and structures of sub-micron size in the bulk glass [1–6]. In silver-containing phosphate glass, the observed fluorescence [1, 7], effective second order [4, 6, 8, 9], and resonant third order [10] nonlinear responses of glass due to the formation of silver-cluster nanostructures (NS) are well appropriate for high resolution optical data storage technologies for instance. In case of axially-symmetric incident laser beam of sufficiently high intensity, the laser-induced evolution of such a material by a train of femtosecond pulses may be described as follows. First, the glass is ionized, which leads to the free electrons absorption of the laser energy, transfer of electron energy to the lattice through collisions, and electron diffusion in the irradiated matter. During the electron diffusion, both mobile electrons and much less mobile holes may be trapped by silver ions to form various silver species. Due to glass heating, the diffusion of these species is thermally-activated leading to silver clusters formation. The latter may be photo-dissociated by subsequent laser pulses in the on-axis region of highest intensities, leading to the formation of ring-shaped silver NS [11]. The associated space charge separation, induced by the metallic species redistribution inside the glass, creates a frozen electric field E_{dc} exhibiting a circular symmetry, which is responsible for both a local centro-symmetry breakdown and the appearance of an effective second order nonlinearity in the tailored glass [4, 6, 9]. The silver clusters also generate absorption bands around 280 nm and 325 nm, inducing a correlative enhancement of 3-photon absorption at 1030 nm [10]. Both nonlinear effects then lead to second and third harmonic generation, SHG and THG, respectively.

The goal of this work is to describe theoretically both SHG and THG formation and evolution processes in laser-irradiated phosphate glasses. The present approach is based on the theoretical model developed in [11], including the above-mentioned processes, where two physical mechanisms have been added to account for experimental observations: (1) temperature-dependent electron diffusion coefficient (2) a pulse-to-pulse decrease in the valence band electron reservoir. The present physical system evolution is first shown to be mainly driven by three main competitive processes, for both the formation of silver clusters and electric field, which timescales are shown to exhibit a scaling law. Based on numerical simulations, we then analyze the evolution of the local nonlinear optical responses as a function of the number of pulses N_p in the train up to 10^4, including spatial profiles for $N_p \leq 1000$. These evolutions are in good agreement with experimentally observed SHG and THG signals, sheding light on the underlying physical mechanisms responsible for the

formation of nonlinear optical properties of the studied glass.

To describe the formation and dissociation of silver clusters, the present model accounts for the laser-induced heating of the glass, diffusion, mobility, and kinetic reactions of laser-induced free charge carriers and silver species. The included kinetic reactions are: (i) the free electron trapping by silver ions $Ag^+ + e^- \rightarrow Ag^0$ resulting in the formation of an intermediate silver species Ag^0 that disappears fastly after each laser pulse due to its high reactivity; (ii) the hole trapping by silver ions $Ag^+ + h^+ \rightarrow Ag^{2+}$; (iii) the first stage of silver clusterization $Ag^+ + Ag^0 \rightarrow Ag_2^+$, that is supposed to be stable. Further clusterization processes are neglected [11]. As input parameters, the model requires the value of free electron and hole densities induced by one laser pulse (n_e^0 and n_h^0, respectively), and the initial density of silver ions $n_{Ag^+}^0$. The diffusion of electrons and their trapping by silver ions lead to a charge redistribution. For a long enough time after a train of laser pulses where recombination and trapping of free charges are significant, the redistributed charge $Q(r)$ depends only on the density of silver ion species, Ag_2^+ and Ag^{2+}: $Q(r) = n_{Ag^{2+}}(r) - n_{Ag_2^+}(r)$. The induced static electric field $\vec{E}_{dc}$ is then evaluated with the Gauss law: $\vec{\nabla}.\vec{E}_{dc} = \frac{Q(r)}{\varepsilon}$ where $\varepsilon = 2.56$ is the static material permittivity. $\vec{E}_{dc}$ leads to an effective second-order susceptibility $\chi^{(2)} = 3\vec{E}_{dc}.\chi^{(3)}$, giving rise to a SHG intensity $I^{SHG} \propto |\chi^{(2)} I_0|^2 \propto |E_{dc}|^2$, where I_0 is the incident laser intensity. The density of silver clusters $n_{Ag_2^+}$ leads to a local $\chi^{(3)}$ enhancement, leading to the resonant THG response [10].

The key model parameters mainly driving the evolution of the present physical system are the kinetic rates of above-mentioned reactions, K_{Ag^0}, $K_{Ag_2^+}$, the electron diffusion coefficient, D_e, and the electron-hole recombination time, τ_{rec}. Due to the lack of experimental data in the specific case of silver-doped phosphate glasses, they have to be estimated through experimental observations. To do so, we construct characteristic timescales of these leading competitive processes which ratios are shown hereafter to provide information on the whole system dynamics. These timescales are τ_{rec}, the electron trapping time $\tau_{trap} = 1/(K_{Ag^0} n_{Ag^+})$, and the electron diffusion time $\tau_{diff} = (l_{diff})^2/D_e$. l_{diff} is a characteristic diffusion length set to 0.1 μm which corresponds to the observed width of the NS, i.e. the spatial scale of charge separation. The smaller τ_{diff}, the stronger the influence of electron diffusion on the final distribution of silver species ($n_{Ag_2^+}$ and $n_{Ag^{2+}}$). In [11], τ_{rec} is set to 150 fs to reproduce the low absorption of the laser-induced free electrons, $D_e = 3 \times 10^{-6}\ m^2 s^{-1}$, and K_{Ag^0} depends on the glass temperature according to an Arrhenius law, where the activation energy is set to 0.8 eV [12]. The kinetic constants of the reactions K_{Ag^0}, $K_{Ag_2^+}$ of the present model are the same as in [11]. However, by using these parameters, E_{dc} reaches values several orders of magnitude lower than as estimated from the experimental efficiency of SHG. To get higher values, the electron diffusion coefficient is then assumed to depend on the lattice temperature T [13]:

$$D_e(T) = D_e(T_0) e^{E_a^e/kT_0} e^{-E_a^e/kT}, \quad \textbf{(1)}$$

where E_a^e is set to 0.55 eV and $D_e(T_0) = 10^{-3}$ m^{2}s^{-1}. It follows that both τ_{trap} and τ_{diff} now depend on T. The experimentally observed density of silver clusters $n_{Ag_2^+}$ is negligible after 100 pulses, meaning that the kinetics are much slower than the charge recombination at $T \approx 300K$, i.e. $\tau_{rec} << \tau_{trap}$. For $N_p = 10^3$, the experimentally observed density of silver clusters $n_{Ag_2^+}$ reaches a significant value of the order of 1% $n_{Ag^+}^0$ [3], with $n_{Ag^+}^0 = 10^{21} cm^{-3}$. In that case, the increase in T during the pulse train leads to the increase of the kinetic rates, leading to $\tau_{rec} \approx \tau_{trap}$, and ultimately $\tau_{rec} > \tau_{trap}$ when the major part of laser-induced electrons are trapped by silver ions and participate to the silver clusterization process. Despite these experimental data do not provide accurate information for $100 < N_p < 1000$, τ_{trap} can be estimated in average. The number of trapped charges during the recombination time multiplied by the number of pulses provides a rough estimation of the cluster density after the pulse train: $n_e^0 \Delta t (1/\tau_{trap} - 1/\tau_{rec}) N_p = 1\% n_{Ag_2^+}^0$, with $\Delta t = min(\tau_{rec}, \tau_{trap})$ and $n_e^0 = 10^{17} cm^{-3}$. So in average over 10^3 pulses, $\tau_{trap} \simeq 0.9\tau_{rec}$. During the pulse train, τ_{trap} then may be even shorter. An efficient charge redistribution takes place if the electron diffusion time τ_{diff} is of the same order of magnitude as τ_{trap}. Based on these estimations, $\bar{K}_{Ag^0} = 7 \times 10^{-9} cm^3 s^{-1}$ and $\bar{D}_e = 7 \times 10^{-2} m^2 s^{-1}$ in average. The latter values allows one to simulate spatial distributions of both silver clusters and E_{dc} similar to the experimental observations. By scaling τ_{rec} by a given factor, the same scaling on all rates of kinetic reactions and D_e leaves the distributions unchanged.

In case of departure from this scaling law, that do not correspond to our experimental observations but which may be appropriate for other conditions (glasses, metal ions, thermal treatment), the system evolution regime may be dramatically different. If $\tau_{rec} \geqslant \tau_{trap} > \tau_{diff}$, the E_{dc} will be directed outwards corresponding to electrons and holes trapped in the periphery and the on-axis region, respectively. If $\tau_{rec} \geqslant \tau_{diff} > \tau_{trap}$, the radial distribution of E_{dc} would exhibit an inner and an outer rings with inwards direction and an intermediate ring with outwards direction corresponding to electrons trapped both in the on-axis region and in the periphery, and holes trapped in the region between them.

The electrons transport may be further influenced with respect to N_p due to the increase in $\vec{E}_{dc}$ which further accelerate the electrons. It is described in the electron diffusion equation by adding a term proportional to the electron drift velocity which reads $\vec{v}_{drift} = \mu_e \vec{E}_{dc}$ (see Eq. (16) in [11]). μ_e is the electron mobility $D_e(T) q_e/kT$ which depends on the lattice temperature according to Eq. (1). Due to this mechanism, the electrons may further compensate the charge separation and reduce strongly E_{dc}. In [11], it was assumed that v_{drift} saturates similarly to the charge carriers drift velocity in semiconductors [14] which maximum value is v_{drift}^{max} = 10 km/s. In the present simulations, the electron diffusion velocity $v_{diff} = D_e/l_{diff}$ also increases with T, and is of the order of 10 km/s for $T = T_0$. It follows that v_{diff} is larger than v_{drift}^{max}, and μ_e can be neglected in the electron diffusion equation. Indeed, the performed simulations show that, if the electron drift velocity does not saturate, E_{dc} is strongly compensated in comparison to the case where the drift velocity saturates to v_{drift}^{max} or if the electron mobility term is neglected. We have checked that there is no significant difference between the static electric field distributions $E_{dc}(r)$ as evaluated in the two cases. In the following, μ_e is thus removed from the modeling and the computational cost of the simulations is then strongly decreased. Nevertheless, we solve the Gauss equation at each numerical time step to account for the compensation of E_{dc} by the mobile silver ions. The mobility of silver ions is

then set to $\mu_{Ag^+} = 2 \times 10^{-16} m^2 s^{-1}$ at T = 528 K to get the best agreement with the experimental observations.

Finally, the previous model has been improved to account for experimental conditions and observation. First, even for a large number of pulses for which the total absorbed energy is large, the melting of glasses has never been observed for pulse energies E_0 smaller than $250nJ$. Previous calculations only accounting for 2D heat diffusion in the plane perpendicular to the propagation axis [11] predict temperatures in excess of the melting point under these experimental conditions. Moving to a 3D analytic expression for the temperature evolution accounting for the geometry of the observed NS [15], values lower then the melting point are retrieved. Second, to be able to work with large number of pulses $N_p > 10^3$, a pulse-to-pulse emptying of the valence band electron reservoir, set to $0.4n^0_{Ag^+}$, is introduced in the modeling. Indeed, a part of free electrons and holes is trapped by silver ions after each laser pulse. Thus, pulse after pulse, the valence-band electron reservoir decreases. The number of produced free electrons n_e^0 then decreases with respect to N_p, leading to a pulse-to-pulse decrease in the induced charge separation per pulse. Such a reservoir evolution may change the pulse-to-pulse laser absorption but, due to the lack of experimental data on the absorption evolution with respect to the number of pulses, it is assumed to remain constant.

Figure 1 shows the radial profiles of the silver cluster density $n_{Ag_2^+}(r)$, charge $Q(r)$, and corresponding $E_{dc}(r)$ for various number of laser pulses N_p going from 30 to 1000 with a repetition rate $\nu = 10MHz$. The pulse parameters are: energy E_0 = 250 nJ, waist a_0 = 1.4 μm, duration $\tau_{FWHM} = 470fs$, wavelength $\lambda_0 = 1030$nm. The calculated value of the absorbed energy is 0.4% of E_0 [11]. Figure 1 also shows the experimentally obtained fluorescence signal (which is proportional to the density of silver clusters $n_{Ag_2^+}$) and the static electric field $E_{dc}^{exp}(r)$ reconstructed from the second harmonic signal $S_{exp}^{SHG}(x)$ for $N_p = 1000$ [4, 8]. The numerically simulated distributions of both quantities are in an overall good agreement with the experimental observations showing the reliability of the present modeling. The position of the outer ring of the reconstructed $E_{dc}^{exp}(r)$ is slightly shifted to the periphery in comparison to theoretical predictions. Such a difference could be explained by diffraction effects occurring in the course of laser propagation along the NS that are not included in the $E_{dc}^{exp}(r)$ reconstruction process. Regarding the evolution of $n_{Ag_2^+}(r)$ with respect to N_p, two stages can be observed: (1) low-density on-axis distribution of silver clusters formed after a small number of pulses (Fig. 1(a) $N_p = 30, 100$) and (2) well-resolved ring NS of silver clusters formed after a sufficiently large number of pulses (Fig. 1 (a) $N_p = 400, 1000$). In the first stage, the ratio between τ_{rec} and τ_{trap} changes dramatically with the temperature T growth from 300K ($\tau_{rec} << \tau_{trap}$) to 400K ($\tau_{rec} > \tau_{trap}$), while the electron trapping and the electron diffusion time scales are comparable in this temperature range: $\tau_{trap} \lesssim \tau_{diff}$. Thus, pulse after pulse, the clusters are created more efficiently, and a strong interplay between electron diffusion and electron trapping takes place. The electron trapping occurs significantly in the on-axis region, where both the density of free electrons and the temperature of the glass are higher than on the periphery of the beam. That provides a faster decrease in the free electron density in the on-axis region. The diffusion of free electrons then creates a flux of electrons not only to the periphery but also in the on-axis region. An accumulation of negative charge in the on-axis region thus occurs during the first

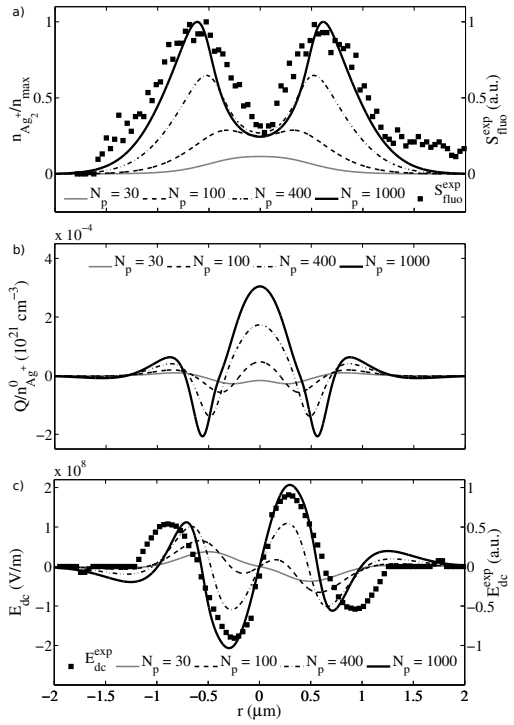

Fig. 1. Evolution of the radial profiles of (a) normalized silver clusters density $n_{Ag_2^+}(r)$, (b) trapped charges $Q(r)$, and (c) frozen electric field $E_{dc}(r)$ for a laser irradiation by 30, 100, 400, and 1000 pulses. The lines and squares correspond to numerical simulations and experimental data, respectively. In (a), clusters fluorescent signal $S_{exp}^{fluo}(r)$ after 1000 laser pulses with 4.53 Jcm^{-2} peak fluence per pulse [4]. In (c), $E_{dc}^{exp}(r)$ is reconstructed from the SHG signal $S_{exp}^{SHG}(x)$ after 1000 laser pulses [4]. Used modeling parameters (see [11] for their definition): $S_0 = 50$; $K_{Ag^{2+}} = 10^{-11} cm^3 s^{-1}$; $K_{Ag^+} = 10^{-10} cm^3 s^{-1}$.

tens of laser pulses (Fig. 1(b) $N_p = 30, 100$). The corresponding frozen electric field E_{dc} is directed inwards (negative values of its amplitude at $r > 0$, Fig. 1(c) $N_p = 30, 100$).

In the second stage corresponding to $\tau_{rec} > \tau_{diff} > \tau_{trap}$, the temperature reaches values above 500K leading to an efficient accumulation of silver clusters. While the density of silver clusters in the on-axis region is growing with the number of pulses, their dissociation rate also increases. According to the chosen dissociation pathway [11], an additional amount of free electrons appears in the on-axis region because of the dissociation of silver clusters, providing a stronger diffusive flux of electrons to the periphery. The accumulation of positive charges then takes place in the on-axis region (Fig. 1(b) $N_p = 500, 1000$), leading to the formation of an inner ring of outwards-directed E_{dc} (represented by positive values at $r > 0$) and shift of the inwards-directed E_{dc} ring to the periphery (Fig. 1(c) N_p = 500, 1000).

The evolution of the SHG and THG signals have been measured during direct laser writing with a pulse train up to 10^4 laser pulses, as shown in Fig. 2 (squares). Such time-resolved in-situ measurements were obtained with a confocal transmission setup with a refractive collection fused silica lens (f = 5 cm, 0.9 NA), two Hamamatsu photomultipliers for the SHG or THG emissions with narrow band-pass filters for each harmonic channel, and a fast oscilloscope (2 Gs/sec, 400 MHz, 1 MΩ impedance). The THG enhancement by silver clusters is

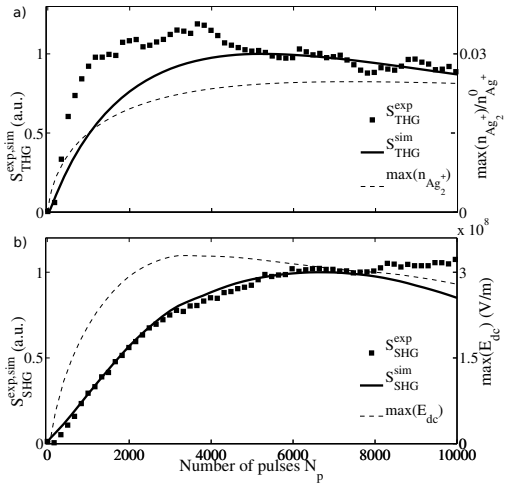

Fig. 2. Evolution as a function of the number of pulses N_p of (a) the normalized experimental and numerically predicted SHG signals S^{exp}_{SHG} and S^{sim}_{SHG}; the maximal value of cluster density $max(n_{A_{g_2^+}})$, (b) the normalized experimental and numerically predicted THG signals : S^{exp}_{THG} and S^{sim}_{THG}; the maximal value of the static electric field $max(E_{dc})$.

interpreted as a near-resonant THG process, leading to the correlative enhancement of 3-photon absorption by silver clusters and THG emission. Under this framework, the THG signal is proportional to the square of the cluster density $n_{A_{g_2^+}}$ since their size is smaller than the laser wavelength [10]. By integrating over space this quantity weighted by the laser pulse intensity in cube $I(\vec{r})^3$, Fig. 2 shows the theoretically predicted evolution of the THG S^{sim}_{THG} with respect to N_p. The agreement with the experimental data is very good, reproducing in particular a maximum value close to 4000 pulses, corresponding to $n_{A_{g_2^+}} = 3\%\ n^0_{Ag^+}$ (Fig. 2 (a) dashed line). The glass temperature drives the cluster density growth which competes with the photo-dissociation process and with the pulse-to-pulse decrease in the density of available valence electrons. When the density of available valence electrons decreases significantly, the amount of clusters created per pulse starts to be lower than the amount of photo-dissociated clusters, leading to a decrease in the total number of clusters and subsequently THG.

Regarding the measured SHG signal, it increases rapidly during the first thousands of pulses, saturates after roughly 10^4 pulses, and then decreases after a few 10^4 pulses. The theoretical prediction S^{sim}_{SHG} is obtained by integrating $E^2_{dc}I^2$ over space. The theoretical trends are in a good agreement with the experimental observations since, predicting the same dynamics for the SHG growth and the existence of a maximum value for which $E_{dc} \approx 3 \times 10^8$ V/m (close to the dielectric breakdown [4], Fig. 2(b) dashed line). Before the reach of the maximum, E_{dc} increases roughly linearly due to the pulse-to-pulse addition of separated charges. The accumulation of heat leading to a glass temperature in excess of 400 K activates the mobility of silver ions, that starts to compensate E_{dc} as early as 2000 pulses. The decrease in the density of available valence electrons with respect to N_p also leads to slow down the E_{dc} growth. Now, the fact that the behavior after large number of pulses ($N_p > 8000$) is not correctly reproduced by the model may be explained as follows. The theoretically predicted S^{sim}_{SHG} decreases after 7000 pulses due to the significant emptying of the valence electron reservoir. The E_{dc} formation then is no longer supported by electron-hole production while the glass temperature reaches 520K and significantly activates the silver ions mobility which compensates E_{dc}. The glass temperature remains close to this relatively high value in our modeling due to the constant value of the absorbed energy per pulse. By decreasing the absorption after 7000 pulses, the temperature drops and remove the ions mobility. The ion compensation is then canceled which leads to a good agreement with the experimental behavior. This observation suggests that further modeling improvements of the absorption efficiency may lead to correct predictions of the SHG up to tens of 10^4 pulses.

In conclusion, a theoretical model has been developed to describe the silver cluster organization into a NS together with the creation of a static electric field inside phosphate glasses induced by a train of fs laser pulses. Up to 1000 pulses, the predicted spatial distribution of both the density of silver clusters and electric field are in a good agreement with experimental data obtained from luminescence and second harmonic generation, respectively. When integrated over space, this modeling is also able to mainly mimic the experimental evolution of both second and third harmonic signals with respect to the number of pulses up to 10^4. Such a comparison has shed light on key physical mechanisms as the pulse-to-pulse emptying of the valence electron reservoir and dependence of the kinetic and diffusion processes on the glass temperature.

This study has been carried out with financial support from the French State, managed by the Conseil Régional d'Aquitaine (MOTIF project). Vladimir Tikhonchuk is acknowledged for fruitful discussions.

REFERENCES

1. M. Bellec, A. Royon, B. Bousquet, K. Bourhis, M. Treguer, T. Cardinal, M. Richardson, and L. CanioniOpt. Express **17**, 10304 (2009).
2. A. Royon, Y. Petit, G. Papon, M. Richardson, and L. CanioniOpt. Mater. Express **1**, 866 (2011).
3. M. Bellec, A. Royon, K. Bourhis, J. Choi, B. Bousquet, M. Treguer, T. Cardinal, J.-J. Videau, M. Richardson, and L. CanioniJ. Phys. Chem. C **114**, 15584 (2010).
4. G. Papon, Y. Petit, N. Marquestaut, A. Royon, M. Dussauze, V. Rodriguez, T. Cardinal, and L. CanioniOpt. Mater. Express **3**, 1855 (2013).
5. E. Janata, A. Henglein, and B. ErshovJ. Phys. Chem. **98**, 10888 (1994).
6. J. Choi, M. Bellec, A. Royon, K. Bourhis, G. Papon, T. Cardinal, L. Canioni, and M. RichardsonOpt. Lett. **37**, 1029 (2012).
7. A. Royon, K. Bourhis, L. Béchou, T. Cardinal, L. Canioni, and Y. DeshayesMicroelectronics Reliability **53**, 1514 (2013). European Symposium on Reliability of Electron Devices, Failure Physics and Analysis.
8. G. Papon, N. Marquestaut, Y. Petit, A. Royon, M. Dussauze, V. Rodriguez, T. Cardinal, and L. CanioniJ. Appl. Phys. **115** (2014).
9. K. Mishchik, Y. Petit, E. Brasselet, A. Royon, T. Cardinal, and L. CanioniOpt. Lett. **40**, 201 (2015).
10. L. Canioni, M. Bellec, A. Royon, B. Bousquet, and T. CardinalOpt. Lett. **33**, 360 (2008).
11. E. Smetanina, B. Chimier, Y. Petit, N. Varkentina, E. Fargin, L. Hirsch, T. Cardinal, L. Canioni, and G. DuchateauPhys. Rev. A **93**, 013846 (2016).
12. O. L. Anderson and D. A. StuartJ. Am. Ceram. Soc. **37**, 1551 (1954).
13. N. Kopidakis, K. D. Benkstein, J. van de Lagemaat, A. J. Frank, Q. Yuan, and E. A. SchiffPhys. Rev. B **73**, 045326 (2006).
14. P. Yu and M. Cardona, *Fundamentals of Semiconductors: Physics and Materials Properties* (Springer, 2010).
15. H. Carslaw and J. Jaeger, *Conduction of Heat in Solids* (Clarendon Press Oxford, 1959).

FULL REFERENCES

1. M. Bellec, A. Royon, B. Bousquet, K. Bourhis, M. Treguer, T. Cardinal, M. Richardson, and L. Canioni, "Beat the diffraction limit in 3d direct laser writing in photosensitive glass," Opt. Express **17**, 10304–10318 (2009).
2. A. Royon, Y. Petit, G. Papon, M. Richardson, and L. Canioni, "Femtosecond laser induced photochemistry in materials tailored with photosensitive agents [invited]," Opt. Mater. Express **1**, 866–882 (2011).
3. M. Bellec, A. Royon, K. Bourhis, J. Choi, B. Bousquet, M. Treguer, T. Cardinal, J.-J. Videau, M. Richardson, and L. Canioni, "3d patterning at the nanoscale of fluorescent emitters in glass," J. Phys. Chem. C **114**, 15584–15588 (2010).
4. G. Papon, Y. Petit, N. Marquestaut, A. Royon, M. Dussauze, V. Rodriguez, T. Cardinal, and L. Canioni, "Fluorescence and second-harmonic generation correlative microscopy to probe space charge separation and silver cluster stabilization during direct laser writing in a tailored silvercontaining glass," Opt. Mater. Express **3**, 1855–1861 (2013).
5. E. Janata, A. Henglein, and B. Ershov, "First clusters of ag+ ion reduction in aqueous solution," J. Phys. Chem. **98**, 10888–10890 (1994).
6. J. Choi, M. Bellec, A. Royon, K. Bourhis, G. Papon, T. Cardinal, L. Canioni, and M. Richardson, "Three-dimensional direct femtosecond laser writing of second-order nonlinearities in glass," Opt. Lett. **37**, 1029–1031 (2012).
7. A. Royon, K. Bourhis, L. Béchou, T. Cardinal, L. Canioni, and Y. Deshayes, "Durability study of a fluorescent optical memory in glass studied by luminescence spectroscopy," Microelectronics Reliability **53**, 1514 – 1518 (2013). European Symposium on Reliability of Electron Devices, Failure Physics and Analysis.
8. G. Papon, N. Marquestaut, Y. Petit, A. Royon, M. Dussauze, V. Rodriguez, T. Cardinal, and L. Canioni, "Femtosecond single-beam direct laser poling of stable and efficient second-order nonlinear optical properties in glass," J. Appl. Phys. **115** (2014).
9. K. Mishchik, Y. Petit, E. Brasselet, A. Royon, T. Cardinal, and L. Canioni, "Patterning linear and nonlinear optical properties of photosensitive glasses by femtosecond structured light," Opt. Lett. **40**, 201–204 (2015).
10. L. Canioni, M. Bellec, A. Royon, B. Bousquet, and T. Cardinal, "Three-dimensional optical data storage using third-harmonic generation in silver zinc phosphate glass," Opt. Lett. **33**, 360–362 (2008).
11. E. Smetanina, B. Chimier, Y. Petit, N. Varkentina, E. Fargin, L. Hirsch, T. Cardinal, L. Canioni, and G. Duchateau, "Modeling of cluster organization in metal-doped oxide glasses irradiated by a train of femtosecond laser pulses," Phys. Rev. A **93**, 013846 (2016).
12. O. L. Anderson and D. A. Stuart, "Calculation of activation energy of ionic conductivity in silica glasses by classical methods," J. Am. Ceram. Soc. **37**, 1551–2916 (1954).
13. N. Kopidakis, K. D. Benkstein, J. van de Lagemaat, A. J. Frank, Q. Yuan, and E. A. Schiff, "Temperature dependence of the electron diffusion coefficient in electrolyte-filled $\mathrm{tio_2}$ nanoparticle films: Evidence against multiple trapping in exponential conduction-band tails," Phys. Rev. B **73**, 045326 (2006).
14. P. Yu and M. Cardona, *Fundamentals of Semiconductors: Physics and Materials Properties* (Springer, 2010).
15. H. Carslaw and J. Jaeger, *Conduction of Heat in Solids* (Clarendon Press Oxford, 1959).